Effects of underrepresented hydrometeor variability and partial beam filling on microwave brightness temperatures for rainfall retrieval

Daniel Harris and Efi Foufoula-Georgiou
St. Anthony Falls Laboratory, University of Minnesota, Minneapolis, Minnesota, USA

Chris Kummerow
Department of Atmospheric Sciences, Colorado State University, Fort Collins, Colorado, USA

Received 24 July 2001; revised 23 January 2002; accepted 4 February 2002; published 5 February 2003.

[1] Cloud models run at 3 km resolution (typical resolution used for microwave radiative transfer applications) apart from ignoring subgrid variability (< 3 km); they also underrepresent variability of cloud particles between the scales of 3 and 15 km. In a previous study by the authors, evidence was presented that neglecting subgrid variability in modeled clouds results in considerable biases in microwave radiance computations. In this paper we present evidence that biases of the same order (−2 to −3 K for 10.7 GHz and + 4 to 5 K for 85.6 GHz) can result from underrepresented variability at scales of 3 – 15 km. In addition, this study reveals significant differences between modeled and observed precipitating fields at the ''edges'' of the storm (regions that border on zero precipitation) and documents the effects that these differences have on radiative transfer computations. It is found that biases due to underrepresented variability within the storm body are of the opposite direction to biases due to ''edge'' effects where partial beamfilling occurs over a field of view, and can counteract to give a misleading overall insignificant bias. However, having these two types of biases present in the (T_b-R) databases (formed by radiative transfer through 3 km modeled clouds) can have a significant effect on rainfall retrievals and can be the source of drastically different and apparently unexplainable biases from region to region and storm to storm. *INDEX TERMS:* 1854 Hydrology: Precipitation (3354); 3359 Meteorology and Atmospheric Dynamics: Radiative processes; 3250 Mathematical Geophysics: Fractals and multifractals; 3360 Meteorology and Atmospheric Dynamics: Remote sensing; 3210 Mathematical Geophysics: Modeling; *KEYWORDS:* rainfall, downscaling, validation variability, beam filling, subgrid

Citation: Harris, D., E. Foufoula-Georgiou, and C. Kummerow, Effects of underrepresented hydrometeor variability and partial beam filling on microwave brightness temperatures for rainfall retrieval, *J. Geophys. Res.*, *108*(D8), 8380, doi:10.1029/2001JD001144, 2003.

1. Introduction

[2] Microwave radiative transfer through precipitating clouds forms the basis of several remote sensing applications, such as precipitation retrieval from passive microwave sensors and assimilation of satellite data in numerical weather prediction models. Thus, care must be exercised in quantifying biases that may result from neglecting or misspecifying cloud/precipitation heterogeneity. In a previous paper, *Harris and Foufoula-Georgiou* [2001] presented evidence that omitting the subgrid variability of hydrometeors in modeled clouds (i.e., variability at scales less than 3 km, which is a typical resolution of cloud models used for microwave radiative transfer), results in considerable biases in microwave radiance field computations. However, cloud models run at 3 km resolution, apart from ignoring subgrid variability, they also underrepresent variability between the scales of 3 km and ∼15 km (as evidenced by *Harris et al.* [2001]). In this study, the effect on microwave radiance field computations of this underrepresented variability is examined. The approach undertaken is akin to that of *Harris and Foufoula-Georgiou* [2001] where stochastic downscaling was used to enhance underrepresented variability to levels of variability seen in observed precipitation fields, and then compare microwave radiance fields of the enhanced product with the original modeled fields.

[3] The larger scales of variability considered in this study necessitated the development of a cascade-based downscaling methodology for enhancement of variability, as an alternative to the wavelet-based methodology used by *Harris and Foufoula-Georgiou* [2001] which can be restrictive if the normalized rainfall fluctuations have broad distributions [e.g., *Perica and Foufoula-Georgiou*, 1996]. Thus the main contributions of this study are: (1) quantification of the effects of underrepresented precipitation variability between scales of 3 km and 15 km on microwave radiance fields and (2) development and validation of a cascade-based conditional simulation (downscaling) scheme

0148-0227/03/2001JD001144$09.00

by which the variability of 3D precipitating clouds produced by numerical cloud models can be enhanced to better match observations. An important step of this work, was the validation of the cascade-based downscaling scheme. For that purpose, a high performance operational numerical weather forecast at 3 km resolution was used, for which coincidental radar observations were also available for validating the statistics and structure of the downscaled rain fields.

[4] This paper is structured as follows. In the next section, description of the numerical weather model, radiative transfer scheme, and specific data sets used for this study is given. Section 3 describes the multiplicative cascade framework developed for downscaling applications with additional details given in Appendix B. Section 4 presents multiplicative cascade parameter estimation results, the downscaling results and validation of the downscaled fields by comparison to NEXRAD radar observations. The effects that the downscaling has on radiative transfer computations are presented and discussed in section 5 and concluding remarks are made in section 6.

2. Model, Radiative Transfer Scheme, and Data Set

2.1. Advanced Regional Prediction System (ARPS) and Forecast Case Description

[5] The numerical model used in this study is the Advanced Regional Prediction System (ARPS) developed at the Center for Analysis and Prediction of Storms (CAPS), University of Oklahoma. The ARPS system incorporates many advances in data assimilation developed at CAPS with particular emphasis on the use of Doppler radar data for model initialization. The ARPS provides daily operational real-time forecasts at horizontal grid resolutions as high as 3 km. Details of the ARPS model are given by *Xue et al.* [1995] (available online at http://caps.ou.edu/ARPS/ARPS4.guide.html). While ARPS is not a model used in the "model bank" of the current TRMM satellite calibration/estimation algorithms, the ARPS microphysics scheme is the same as that used in some of those models. Moreover, since the current "model bank" models are also finite element (as is ARPS) there should not be any essential differences from the general findings in this study if the experiment were repeated with any of those models.

[6] The ARPS forecast model configuration and specific case study used in this paper is identical to that used by *Harris et al.* [2001] and described in greater detail in that paper. The ARPS model forecasted the evolution of a line of convection that developed in eastern New Mexico on 2 June 1999 in response to forcing associated with a well-defined dryline. By 00 UTC on 3 June, the line was located in the western Texas Panhandle and moved slowly eastward until it began to dissipate in western Oklahoma. It is emphasized that the ARPS model is used here in its forecast (rather than generic simulation) mode for the purpose of having concurrent observations to validate the scaling structure of hydrometeors on which the downscaling scheme is based.

[7] While only the fields from the finest (3 km) grid-scale forecast are used in this study, the ARPS forecast was actually configured using three one-way nested computational grids (each with 53 levels in the vertical, with a vertical grid interval that stretched continuously from 20 m at ground to 740 m at an altitude of 20 km). The forecast model used version 4.4 of ARPS and used the six category water-ice microphysical parameterization scheme [*Lin et al.*, 1983]. For specific details on the forecast configuration, including details of data assimilation, the reader is referred to *Harris et al.* [2001].

2.2. Radiative Transfer Scheme

[8] In this study the 3D Monte Carlo radiative transfer scheme of *Roberti et al.* [1994] was used so that the interaction of radiation with neighboring columns and radiant energy leakage from dense areas to surrounding areas [*Liu et al.*, 1996; *Roberti et al.*, 1994] can be adequately modeled (energy leakage refers to the process whereby energy is leaked through the sidewalls of the clouds [e.g., *Liu et al.*, 1996]). The scheme is well documented by *Roberti et al.* [1994] and so is only briefly described here. It is a backward Monte Carlo scheme and cannot treat photons changing polarization state, and thus polarization was not considered in this study. Each 3×3 km^2 cloud pixel was divided into 9 (i.e., 3×3) computational points (i.e., 1 km spacing) and 10^4 photons (regardless of frequency) were started at each computational point for a total of 9×10^4 photons per 3×3 km^2 cloud pixel. Only radiative transfer computations for the emission-based 10.7 GHz frequency and scattering-based 85.6 GHz frequency were performed as these two frequencies have strong correlations to columnar rainwater and ice, respectively.

[9] Absorption, scattering and extinction coefficients were computed directly from hydrometeor contents for cloud ice, cloud water, hail, snow, and rainwater. Cloud species were modeled as 100 micron monodisperse particles/droplets, while hail, snow, and rain were Marshall-Palmer distributed with densities of 0.91, 0.1, and 1.0 g/cm^3 respectively. Radiative transfer computations were performed with nadir-viewing angle allowing a direct comparison between brightness temperature and vertically integrated hydrometeor concentration. The phase function was assumed to be Henyey-Greenstein, the surface was specular (i.e., sea) and the wind speed was set to zero. Note that this last assumption implies that the forecasted storm, which occurred over land, was treated for the purposes of radiative transfer as a storm, which might have occurred over the ocean. This "discrepancy" has no consequence on the results of this study. It would be of essence only if the purpose was to "forecast" the brightness temperatures of this specific storm as it occurred over the Southern Plains of the United States. Rather for our study, a specific storm forecast over land was produced only in order to have concurrent radar observations to validate the scaling nature and parameterization. Insofar as the radiative transfer is concerned, the ARPS forecasted storm was used as any generic storm simulated by any cloud model in order to study the effects of hydrometeor variability on the brightness temperatures.

2.3. WSR-88D Radar Data and Z-q_r Relations

[10] Level II WSR-88D radar data from the Amarillo, TX (KAMA) radar were available for the storm described above from about 22 UTC on 2 June to 01 UTC on 3 June 1999 for purposes of comparison to the model output. Constant

altitude plane position indicator (CAPPI) maps at 1.5 km altitude were made and rasterized at both 3 km and 2 km horizontal resolutions. The procedure used to form the CAPPI and rasterize the polar data is the same as that developed by Alan Seed (Bureau of Meteorology, Melbourne, Australia, personal communication, 1999) and involves a projection of the polar scans onto a horizontal plane, followed by two-times (four-times) oversampling in the azimuthal angular coordinate of the polar projections in order to map the projections to final Cartesian grid for the 2 km (3 km) respectively.

[11] While it is recognized that radar observations do not represent an absolute truth with regards to the measurement of spatial rainfall fields, they are probably the best information we have to date. Errors in radar observations and the processing of these observations to a final rasterized product may have significant effects on establishing the scaling nature and corresponding scaling parameterizations of spatial rainfall. Although some studies [e.g., *Perica and Foufoula-Georgiou*, 1996] have found that inferences about scaling and estimates of the scaling parameters are rather insensitive to the Z-R relationship used to convert radar reflectivities to rainfall intensities, these effects are not well understood and comprise an area needy of further research in the hydrometeorological community [see *Krajewski et al.*, 1996; *Harris et al.*, 1997]. However, in using a scaling structure to represent rainfall fields as was done in this paper, one is reassured from analysis of observations by radars of all types and sizes including the spaceborne TRMM precipitation radar [e.g., *Tessier et al.*, 1993; *Harris et al.*, 2001; *Harris and Foufoula-Georgiou*, 2001], lidar, 2D laser scanners, photogrammetry, and blotting paper (see *Lovejoy and Schertzer* [1995a, 1995b] for a review), that scaling, when it exists, is not overly sensitive to the different error structure of all these sensors.

[12] Rain liquid water content, q_r (in g/m^3), was computed from Z using the Z-q_r relation based on the study by *Ferrier et al.* [1995] after a 53 dBZ upper threshold was imposed to suppress hail contamination and a 20 dBZ lower threshold was imposed to filter out noise and ground clutter. To be consistent, where reflectivity was computed from modeled hydrometeor concentrations, the same relations from *Ferrier et al.* [1995] were used, which also account for reflectivity contributions from snow and hail/graupel. The Z-q_r algorithm also accounted for the temperature allowing a proper representation of the bright band due to melting snow and ice below the melting level.

2.4. General Comparison Between Modeled and Radar Observed Storm

[13] As was discussed by *Harris et al.* [2001] this forecast had phase errors, particularly in the form of a temporal lag. Largely because the NEXRAD data were not available for assimilation at the time of the forecast, the triggering of the storm was delayed in the forecast. In the work by *Harris et al.* [2001] the fields from 3 to 4 hours into the forecast were analyzed. In the present study, the fields 6 to 7 hours into the forecast were chosen for analysis and downscaling. The main reason for this is that for radiative transfer computations, all hydrometeor species were required and in order to downscale them, multiscaling analyses on all species had to be performed (whereas only q_r was analyzed in *Harris et al.* [2001]). Unlike the fields at 3 hours into the forecast, the fields 6 hours into the forecast showed good scaling in the structure function above $\sim$ 18 km and allowed estimation of cascade parameters necessary for the downscaling. This is further discussed in section 4.1.

[14] It is worth briefly comparing the means and peak values of modeled and observed fields. The conditional areal means of a single image of NEXRAD estimated q_r varied from 0.42 to 0.69 g/m^3 over the one hour of radar data used in this study, while that from the modeled fields varied from 1.01 to 1.03 g/m^3. However, NEXRAD estimates may be biased downward slightly due to the hail suppression described in section 2.3, thus comparison of reflectivities may be more meaningful since reflectivities account for precipitating ice which is almost certainly present if reflectivity values are higher than approximately 55 dBZ. The mean areal reflectivities (conditioned once again on $Z > 20$dBZ) were 31–34 dBZ for the NEXRAD observations and 35.3 to 35.5 dBZ for the forecast. Peak reflectivities ranged from 53 to 61 dBZ for the NEXRAD images and 61 to 63 for the forecast images. It is noted that while there are some differences in magnitudes of mean and peak values between modeled and observed precipitation, this does not affect the results of this study which are based on comparison of modeled and downscaled fields, which have the same means.

3. Multiplicative Cascades: Framework and Application to Downscaling

3.1. Analysis Framework

[15] The analysis leading to the estimation of the downscaling parameters is identical to that used by *Harris et al.* [2001], and readers should refer to that paper for greater detail. *Harris et al.* [2001] performed two principal analyses. First, the first-order generalized structure function is computed:

$$S_1(l_x, l_y) = \langle |R(x + l_x, y + l_y) - R(x,y)| \rangle \quad (1)$$

for fields R (representing any one of the hydrometeor species), where x, y denote spatial coordinates and l_x and l_y denote lags in the x and y directions, respectively, and $\langle \ldots \rangle$ denotes the average over all the pairs with lag (l_x, l_y) in an image. $S_1(l_x,l_y)$ is azimuthally averaged about lag $l = \sqrt{l_x^2 + l_y^2} = 0$ to obtain $S_1(l)$ which is tested for scaling or log-log linearity,

$$S_1(l) \sim l^H. \quad (2)$$

The field is then fractionally differentiated by order H, and the moment-scale analysis is performed on the differentiated field. The moment-scale analysis involves computing the moments of the fractionally differentiated field φ,

$$\varphi(x) \sim \frac{\partial^H R(x)}{dx^H} \quad (3)$$

for a range of averaging scales, r (larger r implies lower scale),

$$M_q(r) = \langle |\varphi_r(x,y)|^q \rangle \tag{4}$$

where φ_r represents fractionally differentiated field values at scale r, q is the order of the moment, and $\langle \ldots \rangle$ denotes the average over all the pixels of scale r in an image. Scaling of the moments occurs when

$$M_q(r) \sim r^{-K(q)}, \tag{5}$$

where $K(q)$ is the moment scaling exponent function that, in practice, is estimated by log-log linear regressions of the qth moment of $|\varphi_r|$ versus r. Clearly, $K(1) = 0$ since the unconditional mean of the entire field is scale independent. While only $q = 2$ was considered by *Harris et al.* [2001] to demonstrate the presence of scaling, the entire $K(q)$ function is needed here in order to estimate scaling parameters to be used in the downscaling scheme.

[16] There is a rich literature, which defines analytical forms of the function $K(q)$ for multiplicative cascades with certain random generators. For example, a multiplicative cascade with lognormally distributed weights can be shown to have a $K(q)$ function that is a parabola, intersecting the abscissa at $q = 0$ and $q = 1$, and the curvature of the parabola is defined by the log variance of the lognormal distribution from which the multiplicative weights are drawn. The formulation for the derivation of these analytic forms lies in Taubian theorems of probability theory [e.g., *Feller*, 1966]. In this work, the cascade model adopted has log stable distributed weights, also referred to as a universal multifractal [e.g., *Lovejoy and Schertzer*, 1995a, 1995b; *Tessier et al.*, 1993; *Pecknold et al.*, 1993; *Wilson et al.*, 1991]. The subject of stable distributions is, in itself, extensive [e.g., *Samorodnitsky and Taqqu*, 1994], and the derivation is beyond the scope of this work. For a log stable cascade, $K(q)$ is a function of two parameters (see *Harris* [1998] for a derivation)

$$K(q) = \frac{C_1}{(\alpha - 1)}(q^\alpha - q), 0 < \alpha \leq 2, \alpha \neq 1. \tag{6}$$

C_1 is the intermittency parameter and α is the Levy index, ($\alpha = 2$ indicates a lognormal cascade). While C_1 can be simply computed directly as $\partial K(q)/\partial q|_{q=1}$ (L'Hopital's rule), α can only be found by nonlinear regression of (6) to the empirical $K(q)$ curve found from the moment-scale analysis (equations (4) and (5)). Thus C_1 and α are usually estimated together as a pair in the nonlinear regression. Regression is complicated by the fact that scaling for low q (i.e., $q < 0.75$) can be poor due to measurement noise contamination, the presence of zeros, and measurement sensitivity which can cause small nonzero values to be read as zeros [*Harris et al.*, 1996, 1997], while for arbitrarily high q, $K(q)$ becomes linear with the slope depending on the single highest values in the field on which the moment-scale analysis is performed [e.g., *Harris et al.*, 1996, 1997]. Thus (6) only applies to a finite range of q when considering a finite amount of data with measurement artifacts. A routine for robustly estimating $K(q)$ parameters and the q-limits to which it applies was developed by *Harris et al.* [1997].

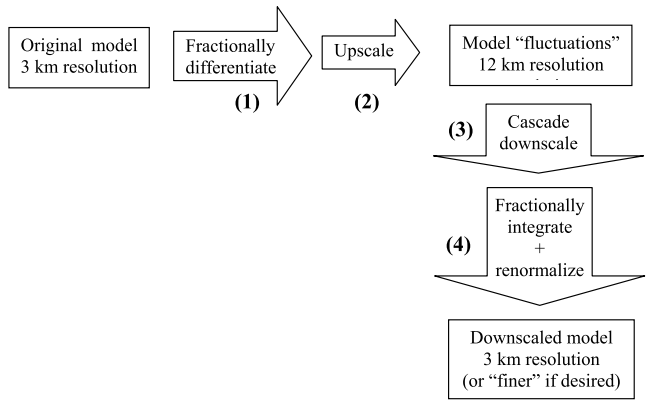

Figure 1. Schematic of the upscaling/downscaling procedure. Each vertical level is done independently but keeping the same random seed. The effects of this simplification are minor and discussed by *Harris and Foufoula-Georgiou* [2001]. (1) Fractionally differentiate the original field using the slope, H, of the first-order structure function as the order of differentiation. (2) Upscaling (horizontal averaging) of the fractionally differentiated modeled fields. (3) Downscaling using a cascade with the cascade parameters found in section 4.1 The number of steps in the cascade determines the final resolution. (4) Fractionally integrate the field and renormalize over the entire cloud to ensure that the total mass of a specific hydrometeor species is conserved.

[17] As discussed by *Harris et al.* [2001], the parameters H, C_1, and α have physical interpretations as indicators of smoothness, intermittency and spikiness, respectively and an illustrative discussion is included in Appendix A. It should also be noted that the parameter H has a dual function as the order of fractional differentiation in the analysis as well as an indicator of smoothness. Fractional calculus is a rich area of study [e.g., *Hilfer*, 1997; *Gorenflo and Mainardi*, 1998, and references within] from which one can show how fractional differentiation and integration can be implemented via power law filters in Fourier space [*Harris et al.*, 2001; *Schertzer and Lovejoy*, 1987]. Fractional differentiation with $H = 0$ would imply no differentiation at all, while $H = 1$ would imply usual differentiation. As seen in the work of *Harris et al.* [2001], H for q_r lies somewhere in between, thus requiring fractional differentiation. As noted elsewhere [*Tessier et al.*, 1993], the results of the moment-scale analysis are not overly sensitive to the order of fractional differentiation, H. However, this is not to mean that H is not an important parameter when it comes to downscaling, where H is an important and sensitive parameter characterizing the smoothness (and thus variability) of the field being downscaled. It is only in the analysis that the specific value of H used has little effect on the outcome of the moment scaling parameters, C_1 and α.

3.2. Downscaling

[18] The schematic in Figure 1 illustrates the steps comprising the downscaling procedure. The procedure requires the three parameters described above: the fractional differentiation and integration parameter, H, and the two

Table 1. Forecast Model Scaling Parameters for 3 June 1999[a]

Field[b]	H	$C1$	α
q_r	0.28 ± 0.02	0.36 ± 0.04	1.1 ± 0.1
q_h	0.29 ± 0.02	0.40 ± 0.04	1.5 ± 0.2
q_s	0.61 ± 0.02	0.21 ± 0.04	1.1 ± 0.2
clw	0.22 ± 0.02	0.41 ± 0.04	0.8 ± 0.1
ciw	0.25 ± 0.02	0.30 ± 0.04	1.3 ± 0.2

[a]Scaling exponents are computed for scales larger than the scale at which the falloff in spectral power occurs ($\sim 5\Delta x$, where Δx is the grid scale of the numerical model and for this forecast is 3 km).

[b]Here q_r, rain liquid water; q_h, precipitating ice (hail, graupel); q_s, snow; clw, cloud liquid water; ciw, cloud ice. All fields are in g/m^3.

cascade parameters, C_1 and α. There are some technicalities in the downscaling procedure, which require some explanation and are given in Appendix B. The technicalities address two issues that were encountered in developing the downscaling methodology using multiplicative cascades. The first issue is that rain fields, whether modeled or observed, contain a substantial number of zeros, while the cascades referred to in section 3.1 do not contain zeros. Clearly the zeros are important to both the spatial and temporal structure of rainfall and this makes the use of discrete cascades employed here, a more suitable choice than continuous cascades [e.g., *Pecknold et al.*, 1993], which generate an additive field in log space and then exponentiate it. Also, the process of fractional differentiation and integration can introduce a field offset (introduced by the power law filtering in Fourier space), which effectively removes all the zeros. It is important to ensure that large areas of zeros (i.e., larger than the scale defining the upper limit of scaling), remain zeros when downscaling. The method described in Appendix B ensures this. The second issue is that real rainfall (unlike a multiplicative cascade) does not usually scale over the entire range of observable scales. In this case, care must be taken not to affect the largest scales beyond which scaling is not observed. For instance the power spectrum of the observed rainfall in this study and that of *Harris et al.* [2001] showed scaling up to $\sim$50 km. Since fractional integration and differentiation affects the entire range of scales, the fractional integration and differentiation filter has to be modified to only affect the smaller scales. This modification is described in Appendix B.

4. Results and Validation of the Downscaling

4.1. Downscaling Parameter Estimates

[19] The parameters used for the downscaling were obtained from the radar observations for rain liquid water, q_r, and from the original modeled fields for the other four hydrometeor species (since no reasonable estimates of these can be made from the radar). The decision to use scaling parameters from the radar observed field instead of the modeled field for q_r, was made on the principle of using real observations where available. In the future it would be desirable to carry out a study of this type using a high resolution model forecast of a storm which was observed intensively with aircraft measurements of cloud water concentrations and high resolution multiparameter radars able to distinguish liquid rainwater, snow and precipitating ice. Thus, in the absence of measurements, the scaling observed at larger scales in the modeled ice particle fields is simply extrapolated down to smaller scales. The basis for this approach is that previous studies on the spatial structure of nonprecipitating particles largely by in-situ (aircraft) measurements [e.g., *Davis et al.*, 1996; *Lovejoy and Schertzer*, 1995b] have shown a scaling structure. This historical basis together with the known issue that the variability of scalar fields in finite element modeled fields is necessarily underrepresented forms the overall justification for this approach.

[20] The scaling parameters obtained from the radar estimated q_r fields were $H = 0.48 \pm 0.03$, $C_1 = 0.26 \pm 0.02$, and $\alpha = 1.4 \pm 0.2$ and the scaling range was from 2 km to 128 km. The scaling parameters obtained from the original ARPS forecasted hydrometeor fields are all listed in Table 1. For the ARPS model scaling parameters, the scaling range was from 12 km to 192 km (the cloud ice and snowfields showed scaling up to 384 km due to their broader horizontal extent). So when comparing scaling parameters of the ARPS model to the radar scaling parameters, one has to keep in mind that ARPS scaling parameters are only defined for scales above 12 km, whereas radar scaling parameters are defined down to scales as small as 2 km.

[21] Much information can be gathered from Table 1. First, it is noted that the modeled q_r field has a higher intermittency parameter, C_1, than the observations (0.36 versus 0.26) but a lower value for α (1.1 versus 1.4) i.e., the modeled q_r field is less spiky. The reason for why the model is showing higher intermittency can be linked to a feature of the modeled field, which is not as predominant in the observed fields. This feature is a frequent presence of abrupt edges in the forecasted field where intense areas of precipitation border areas of no precipitation (see Figure 2). While such features are observed in real precipitation, the model seems to have an unusually high occurrence of such abrupt edges and will be shown later to have an important impact on the radiative transfer results. Thus using the

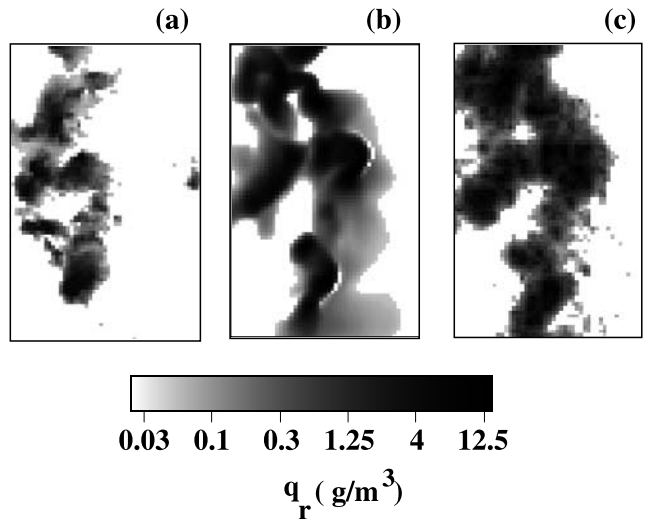

Figure 2. (a) Radar estimated rain liquid water, q_r, at the ground, (b) original ARPS forecasted q_r, at the ground, and (c) downscaled ARPS forecasted q_r at the ground. All images are at 3 km resolution and over an area of 240 × 150 km^2.

scaling parameters of the radar rather than modeled q_r fields was a good choice in this case.

[22] The ARPS snowfield showed the lowest intermittency (lowest C_1) and highest degree of smoothness (highest H). Also the two ice species (cloud ice and precipitating ice) were found to be the spikiest fields (highest α), while the cloud liquid water had the lowest degree of spikiness (lowest α). Again, there is no certain way to suggest if these are reasonable features, given radar observations alone. However, 1D horizontal transects (aircraft mounted probe measurements) of cloud liquid water from scales of 10 m to ~20 km were analyzed by *Davis et al.* [1996] and resulted in C_1 being generally below 0.15 and H between 0.22 and 0.37 for cloud liquid water in marine stratocumulus clouds, which one would expect to be less intermittent than clouds of mid-continental convective systems. Using a similar type of data, *Lovejoy and Schertzer* [1995b] found 1D cloud liquid water paths to have H = 0.28, C_1 = 0.07, and α = 2.0 (i.e., lognormal), which is much spikier than any field encountered in this study, although the reported high value of α could be an artifact of the inability of the liquid water probe to measure very low concentrations (S. Lovejoy, McGill University, personal communication, 2001).

4.2. Downscaling Results and Validation

[23] Examples of original modeled and downscaled modeled q_r fields are shown in Figure 2, along with an example of the radar data. Note that the modeled fields show a greater horizontal extent compared to the observed fields, but this does not affect the results of this study as comparisons of radiative transfer are done between the original ARPS (Figure 2b) and downscaled ARPS (Figure 2c) fields. From Figure 2, one can visually see that the original modeled field looks smoother than the radar observations while the downscaled field looks more like the radar observations. To further quantify this some relevant one-point statistics (such as the coefficient of variation) and two-point statistics (such as power spectra and other multiscale measures) were computed for the observed, original model and downscaled model fields. Since only radar observations were available only rain liquid water, q_r, and reflectivity, Z, could be validated. Validating Z as opposed to q_r has the advantage that Z includes precipitating ice and does not require radar-estimated q_r to be thresholded for hail suppression. One-point and two-point statistics were computed for both Z and q_r and results did not differ greatly so only the analysis of the Z fields is presented below for conciseness. Note that the analyses were performed on the Z fields in mm^6/m^3 and not the (logarithmic) dBZ fields.

[24] Figure 3 shows the mean coefficient of variation (CV) of q_r for pixels within boxes of varying sizes (seen as satellite fields of view (FOV)). The TRMM instrument has varying effective FOVs (EFOVs) depending on the frequency of the channel, ranging from 35 km^2 for the 85.6 GHz channel to 2300 km^2 for the 10.7 GHz channel [*Kummerow et al.*, 1998], and corresponding to "box" sizes of 6 km and 48 km, respectively. Only boxes having at least six nonzero values were included in the computation, in order to have a meaningful sample size. While somewhat arbitrary, six nonzero values was found high enough to ensure sensible statistics calculations and follows the radar rainfall statistics study by *Matrosov and Djalalova* [2001]. Figure 3 shows how the downscaling increases the mean CV of the original model to values comparable to those estimated from the radar data.

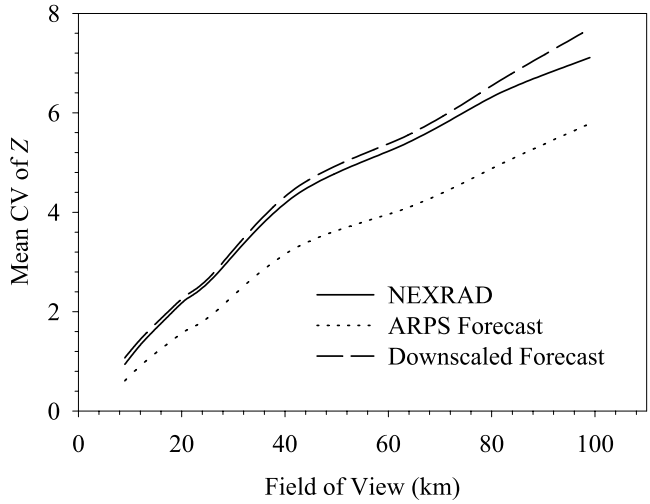

Figure 3. Comparison of variability (as measured by the coefficient of variation (CV)) of NEXRAD observations, ARPS forecast, and the upscaled/downscaled forecast all at 3 km resolution for reflectivity, Z, in mm^6/m^3. The graph shows how downscaling increases the variability of the original forecast and brings it close to the variability of the observed field.

[25] The CV value within a specific box size is generally dependent on the mean value of q_r in that box. Figure 4 shows the distribution of CV values within 21 km boxes for different ranges of the mean q_r. The largest differences between radar and original forecasted fields are seen for low to moderate intensities of rainfall with mean q_r between 0.05 and 0.4 g/m^3. The variability of boxes with more intense rainfall is seen to agree. Likewise, the downscaling is shown to greatly increase the variability for low to moderate rainfall, while having less effect on heavier rainfall. It is noted that for the CV analysis, the radar fields at 2 km were regridded to the 3 km resolution of the ARPS forecasts for a fair comparison of their statistics at the same scale. For the multiscale analyses that follow such a regridding is not necessary since statistics over a range of scales are computed and compared.

[26] The analysis leading to Figures 3 and 4 showed that the downscaling properly enhances the variability (as measured by the CV), which is lacking in the original modeled fields. However, the spatial correlation structure of the modeled precipitation is important as well for radiative transfer computations (see Appendix C). Thus it is imperative that the downscaling produces a realistic spatial correlation structure in addition to a realistic degree of variability. To test this, two-point statistics must also be validated. *Harris and Foufoula-Georgiou* [2001], and *Harris et al.* [2001], used the Fourier power spectrum as the principal two-point statistical measure as rainfall often has a structure yielding scaling power spectra [e.g., *Harris et al.*, 1996; *Menabde et al.*, 1997;

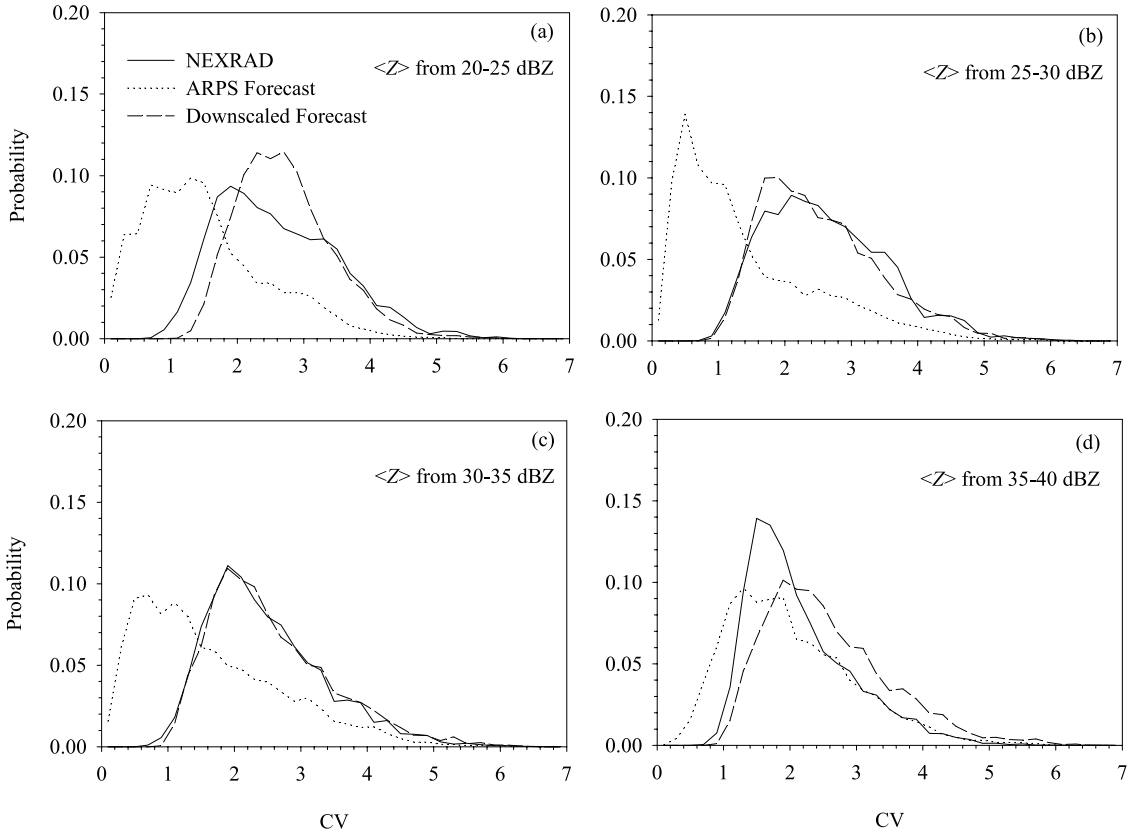

Figure 4. Coefficient of variation (CV) distributions for 24 × 24 km^2 boxes with (a) $\langle Z \rangle$ between 20 and 25 dBZ, (b) $\langle Z \rangle$ between 25 and 30 dBZ, (c) $\langle Z \rangle$ between 30 and 35 dBZ, and (d) $\langle Z \rangle$ between 35 and 40 dBZ. Note that downscaling helps bring the ARPS forecast distributions close to the distributions of the NEXRAD observations, validating the downscaling methodology.

Lovejoy and Schertzer, 1995a; *Georgakakos et al.*, 1994]. A scaling power spectrum for the observed radar field was also found in this study as seen in Figure 5. However, the original modeled field had a sharp fall off in the tail end of the spectrum at wave numbers greater than about 0.06 – 0.07 which corresponds to ~ 15 km, or five times the model grid resolution. This fall off in the spectra of modeled precipitation fields was documented by *Harris et al.* [2001], and is a result of implicit and explicit numerical diffusion in finite difference computational fluid dynamical (CFD) models. In line with the primary incentive of using the cascade framework to enhance the variability of the original modeled fields, the spectrum of the upscaled/downscaled field shows scaling and effectively has increased "energy" at higher wave numbers (as observations do), relative to the original modeled field (see Figure 5).

[27] The multiscale analyses described in section 3 were also applied to the NEXRAD, original ARPS and downscaled ARPS fields. Figure 6 shows the first-order structure function, the second-order moment-scale analysis, and $K(q)$ curve for all three fields. The results corroborate the finding that downscaling properly enhanced the variability and spatial structure of the forecasted fields to bring it closer to the structure of the observed fields. For example, Figure 6a shows how the fall off in the small-scale end of the curve for the original forecasted field (indicating smoothness) was

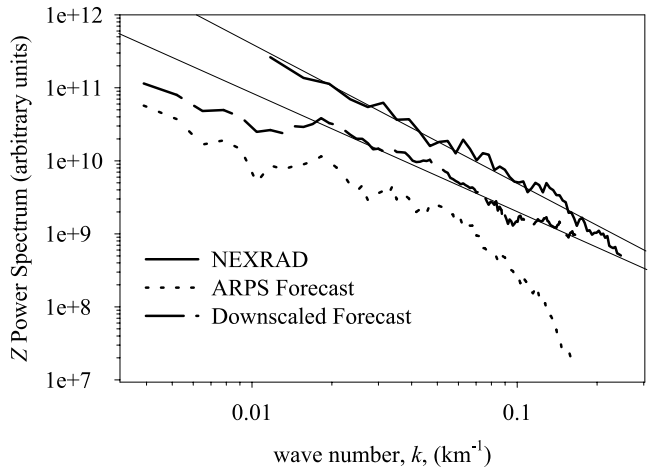

Figure 5. Power spectra of reflectivity, Z, for NEXRAD radar, and computed Z (see section 2.3) for the original, and downscaled forecasted fields. The radar field is at 2 km resolution while the forecasted fields are at 3 km resolution. The plot shows how the fall off in the tail of the original forecasted field, which indicates smoothness, is removed by the downscaling. Spectra are vertically displaced for clarity.

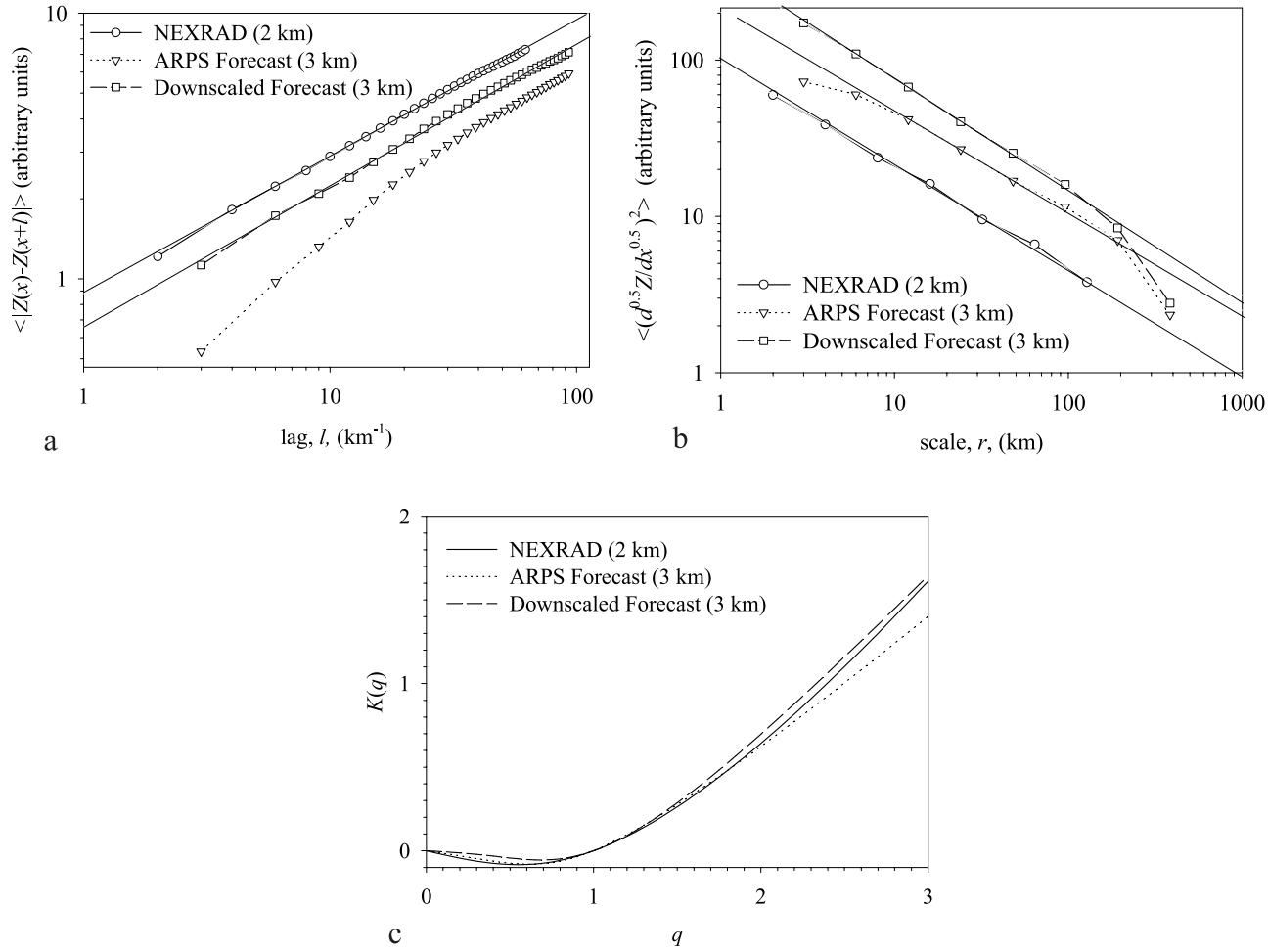

Figure 6. (a) First-order (q = 1) generalized structure functions, (b) second-order (q = 2) moment scale analysis, and (c) $K(q)$ curves for NEXRAD observed, original ARPS, and downscaled ARPS computed radar reflectivity, Z, near the ground. The radar field is at 2 km resolution while the forecasted fields are at 3 km resolution.

removed by the downscaling, while Figure 6b shows how the leveling off in the small-scale end of the curve for the original forecasted field (indicating homogeneity or lack of intermittency) was removed by the downscaling. The $K(q)$ curves in Figure 6c demonstrate that downscaling brought the higher-moment variability ($q > 2$) of the original ARPS forecast closer to that of the NEXRAD observations. Of course, this was helped by the fact that the downscaling parameters were estimated from the radar (not the ARPS forecasted) fields and point out the need to have observations from other species too for parameter estimation, as one might get from a meteorological intensive observation period (IOP) field campaign.

[28] A final but important feature to consider, was mentioned in section 4.1 and refers to the sharp and abrupt edges in precipitation fields. By sharp and abrupt edges, we mean the occurrence of very intense rainfall bordering on regions where it is not raining at all (i.e., on the borders of the storm's outline). This is apparent in Figure 2 where one sees that the model shows a more frequent occurrence of such edges than the observed fields. To quantify the extent of this feature, a histogram was computed of the 3 km reflectivity values within 24 × 24 km^2 FOVs that are bordering on the storm's outline. An FOV is considered bordering on the storm's edge if the FOV consisted of approximately two-thirds nonraining pixels (for computational purposes this was expanded to include 10% either side of two thirds to gain good statistics). These FOVs are termed here "partial beamfilling" FOVs. The histogram of reflectivity values for such FOVs for which the mean reflectivity over the entire FOV was greater than 45 dBZ is shown in Figure 7a for the observed, original, and upscaled/downscaled modeled fields. The histogram shows a pronounced peak in reflectivities between 50 – 60 dBZ for the original forecast that is not present in the histograms of the observed or downscaled fields. The effect of these abrupt edges is very high variability (high CV) in these FOVs for the original ARPS forecast as shown in Figure 7b by the histograms of the coefficient of variation (CV) for the data in Figure 7a. If anything, the downscaling slightly underrepresents the frequency of occurrence of such abrupt edges in comparison to the radar observed fields. This can be seen in Figure 7a and 7b where the downscaled field shows both the lowest frequency of high intensity precip-

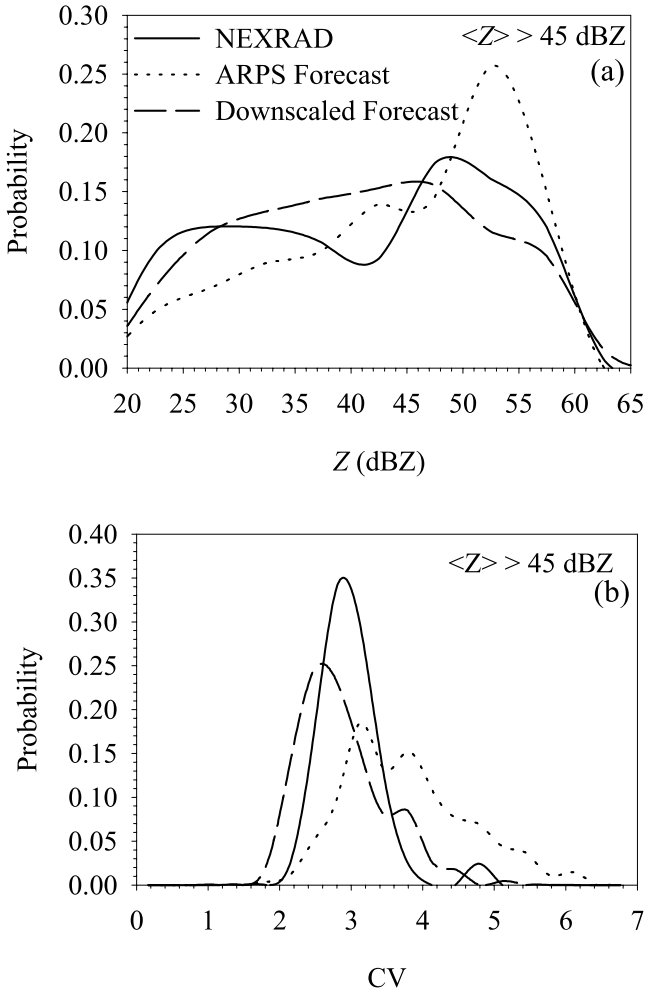

Figure 7. Histograms of (a) 3 km reflectivity values and (b) coefficient of variation (CV) within 24 × 24 km^2 FOVs with mean reflectivity greater than 45 dBZ, that are bordering on the storm's outline (i.e., suffer from partial beamfilling). An FOV is considered bordering on the storm's edge if the FOV consisted of two-thirds nonraining pixels. The large peak between 50–60 dBZ for the original ARPS forecasted field is indicative of higher occurrences of intense precipitation on the edges of the storm in comparison to observed NEXRAD fields and the upscaled/downscaled forecasted fields.

itation ($Z > 45$ dBZ) and the lowest CVs for FOVs suffering from partial beamfilling.

5. Effect on Radiative Transfer

[29] Radiative transfer computations were performed using the scheme described in section 2.2, and comparisons were made between brightness temperature fields for the original ARPS and upscaled/downscaled 3 km forecasts. Comparisons are presented here for 24 × 24 km^2 FOVs. Figure 8 shows an example of T_b versus vertically integrated rain liquid water for 10.7 GHz radiance fields of the original and downscaled fields for FOVs containing no zeros (FOVs inside the body of the storm). As is the norm, the scatter is great and a third-order polynomial regression of the data is superimposed. While no importance is attached to the actual fit, the regressions provide a visual aid to assess the bias between the downscaled and original radiance fields. The curves were not very sensitive to the order of the polynomial used in the regression providing it was greater than second-order, and show the bias to increase with q_r. Equally important is that the curve for the downscaled forecast is seen to lie below that of the original forecast consistent with the normal trend of cooler temperatures for increased variability. When all 24 × 24 km^2 FOVs were considered (instead of only the fully covered FOVs), a plot similar to that of Figure 8 was obtained. The scatter is too large to allow a quantitative assessment of the biases.

[30] To obtain a quantitative assessment of the biases we consider an approach whereby one is essentially taking vertical "slices" of the data in Figure 8 for certain ranges of vertically integrated q_r, and plotting the distributions of T_b for a specified range of q_r values. Figure 9 shows the distribution of 10.7 GHz T_b values for two ranges chosen to represent moderate columnar q_r (5 – 10 g/m^2) and high columnar q_r (greater than 10 g/m^2). A number of conclusions can be drawn from Figure 9. First, comparison of Figures 9a and 9b computed for the entire field corroborates what was seen in Figure 8, namely, that the magnitude of the mean biases (−1.4 K and −5.7 K for moderate and high q_r, respectively) increases with precipitation intensity. In order to illustrate the effect on radiative transfer of the frequent occurrence of abrupt edges in the original ARPS forecast (as illustrated by Figure 7), distributions for each of the two ranges in Figures 9a and 9b were recomputed for FOVs that do not include any regions of zero columnar q_r, so as to exclude the effect of partial beamfilling at the storm's edges. These results are shown in Figure 9c and 9d. It is apparent here that high columnar q_r distributions were hardly affected by restricting FOVs to contain no zeros as high q_r values are not, in general, partially filled (which is why they are high). For moderate columnar q_r, however, the effect is more significant with increasing change of bias from −1.4 K to −3.7 K.

[31] Table 2 provides a summary of the effects illustrated in Figure 9 by listing the mean T_b biases over all FOVs (B), over FOVs completely covered by rain ($B_{nonzero}$), and over FOVs with partial beamfilling (B_{edge}). The bias of the scattering-based 85.6 GHz channel is expected to be in the

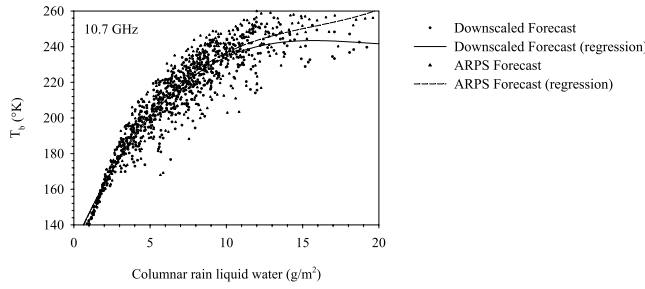

Figure 8. T_b versus q_r for the 10.7 GHz frequency for the downscaled (dots) and original forecast (triangles). T_b are for 24 × 24 km^2 FOVs containing no zeros. Third-order polynomial regressions were fit and included to aid visualizing the trend in bias, where the dashed line represents the original forecast and the solid line represents the downscaled forecast.

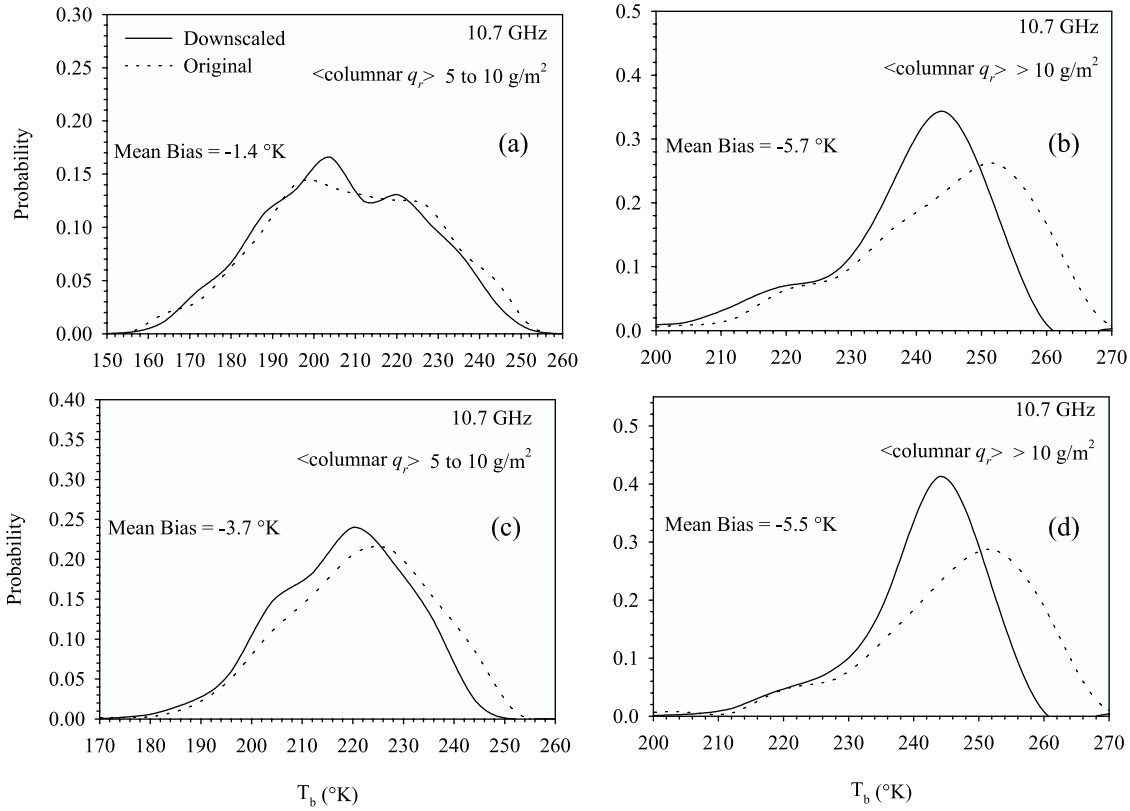

Figure 9. Distributions of brightness temperatures for two ranges of vertically integrated (columnar) q_r, representing mid-range columnar q_r (5 to 10 g/m^2) and high range q_r (> 10 g/m^2). T_b values are for 24 × 24 km^2 over all FOVs (top two plots) and over FOVs that do not contain any zeros (bottom two plots). FOVs on ''edges'' are not likely to be associated with high q_r due to the presence of zeros, thus Figure 9b and 9d show similar biases. However, for medium range q_r values, FOVs with partial beamfilling are seen to create a positive bias of approximately +2 K, which reduces the bias coming from the body of the storm from −3.7 K to an overall bias of −1.4 K.

opposite direction to the emission-based 10.7 GHz channel as a result of the tendency of T_b to decrease with increased precipitation for the 85.6 GHz channel, whereas the 10.7 GHz channel yields T_b that increase with increased precipitation [*Kummerow*, 1998]. The impact of the edges is seen to be significant if one compares B to $B_{nonzero}$. To further confirm that edges were indeed the primary cause of this, biases were computed for edge pixels alone (accounting for ∼20% of the total number of FOVs) and listed in Table 2 as B_{edge}. As expected the biases for these FOVs suffering from partial beamfilling, were in the opposite direction to the overall biases and to biases coming from fully covered FOVs. Considering that the variability within the body of storm was well treated by the downscaling (as evidenced by the validation), while the treatment of the storm edges showed signs of overcorrecting for the excessive frequency of intense and coherent edges in the forecasts, the results in Table 2 imply that the true overall biases lie somewhere between the reported values of B and $B_{nonzero}$.

6. Summary and Conclusions

[32] Microwave rainfall retrievals based on radiative transfer computations through modeled precipitating clouds greatly depend on the ability of the numerical cloud models to properly capture the natural variability of hydrometeor species. In a previous study [*Harris and Foufoula-Georgiou*, 2001], evidence was presented that ignoring variability at scales below the typical resolution of cloud models (< 3 km) induces significant biases in T_b of approximately −2 K for 10.7 GHz and +5 K for 85.6 GHz. Cloud models run at 3 km resolution, apart from ignoring variability at scales less than 3 km, they are also known to underrepresent the variability between 3 km and ∼15 km [e.g., see *Harris et al.*, 2001].

[33] In the present study the issue of how well cloud models represent variability between scales of 3 km and 15 km, was further considered and the effect of underrepresented variability on radiative transfer computations was examined. In addition, a cascade-based downscaling methodology was developed for the purpose of stochastically enhancing the underrepresented variability of the modeled fields to levels close to those found in observed fields. Considerable attention was paid to validating the down-

Table 2. T_b Mean Biases[a]

f, GHz	B, K	$B_{nonzero}$, K	B_{edge}, K
10.7	−0.2	−4.7	+2.7
85.6	−1.9	+4.8 (+7.9)	−3.1

[a]Note: B is the mean bias over all FOVs, $B_{nonzero}$ is the mean bias over FOVs completely covered by rain, and B_{edge} is the mean bias over FOVs with partial beamfilling defined as consisting of ∼2/3 zeros. The number in parenthesis indicates the bias when conditioned on graupel/hail fields.

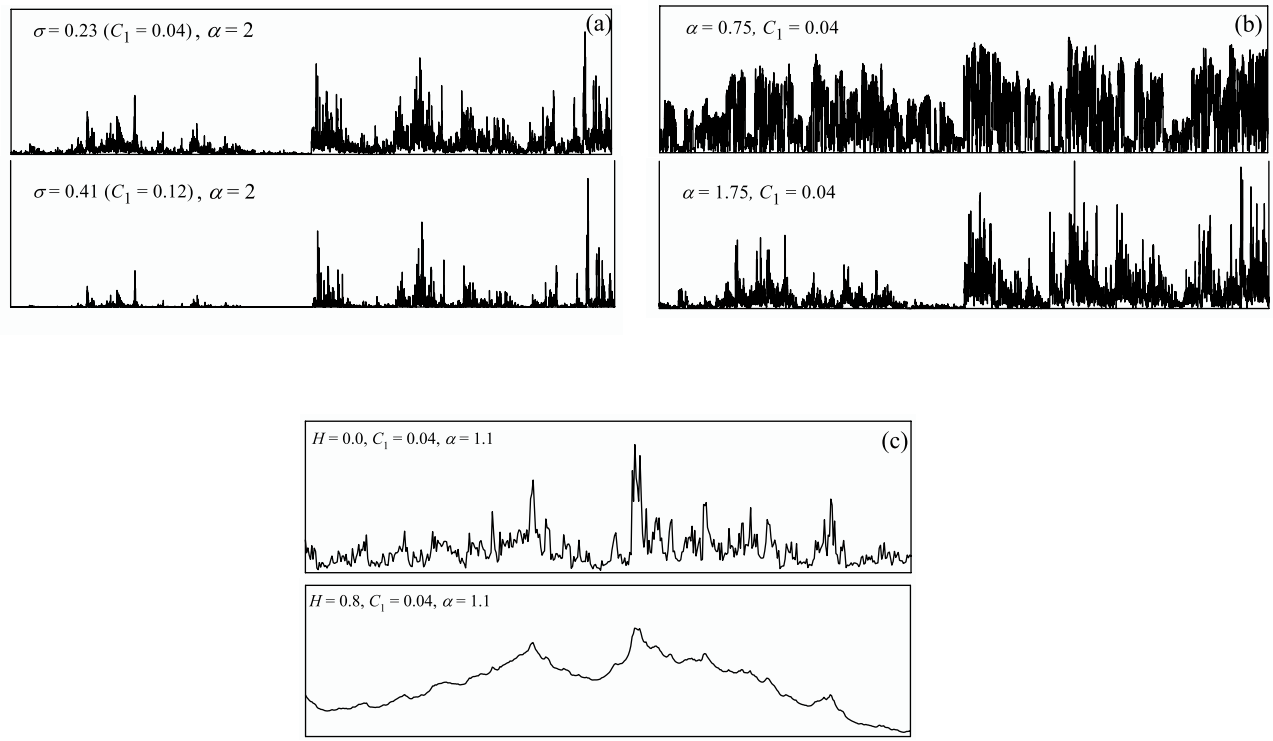

Figure A1. Examples of simulated intensities using cascade models with varying parameters: (a) $\alpha = 2$ (lognormal) cascades with varying intermittency parameter C_1 (or equivalently, the stable scale parameter, σ, where $C_1 = \sigma_2/2\ln b$ [*Harris*, 1998]), (b) log stable cascades with varying α for fixed $C1$, and (c) log stable cascades with fixed α and fixed C_1 but varying H. For each pair, the two cascades are generated with the same initial seed required by the random generator making them look similar except for the intermittency. In Figure 10a increasing intermittency, implies concentrating more mass into sparsely distributed intense bursts. In Figure 10b increasing α implies a field that is more spiky. The terminology introduced by *Schertzer and Lovejoy* [1992] refer to multifractal processes with $\alpha < 1$ as soft and processes with $\alpha > 1$ as hard. In Figure 10c, increasing H implies a field that is smoother. Technically, H is the degree which a field is fractionally integrated (hence the increasing smoothness).

scaling methodology. For that purpose, a state-of-the-art numerical weather forecast (provided by the Advanced Regional Prediction System (ARPS)) initialized for a specific real event was chosen so that coincident radar observations could permit a validation of the downscaling scheme. The validation analysis further documented the shortcomings of numerical cloud models to represent small-scale variability [*Harris et al.*, 2001; *Harris and Foufoula-Georgiou*, 2001]. It also demonstrated the ability of the proposed cascade-based downscaling methodology to properly enhance the statistical structure of the original modeled fields and produce fields with similar variability, spatial correlation and multiscaling structure as the radar observations.

[34] A significant issue pointed out by the validation analysis is that the 3 km forecast fields have much more coherency than the observed precipitation fields (as evidenced by their much smaller CVs) and a higher occurrence of intense (high precipitation) coherent structures bordering on regions of zero rainfall (edges of the storm). The effect of these coherent structures at the storm edges is high CVs in any FOV that partially covers such coherent structures (FOVs with partial beamfilling). As a result, radiative transfer computations for these FOVs result in considerably cooler temperatures for 10.7 GHz (warmer temperatures for 85.6 GHz) than FOVs with similar mean precipitation that do not suffer from partial beamfilling (i.e., within the body of the storm). These cooler temperatures due to partial beamfilling for the ARPS forecast counteract the general trend of warmer temperatures within the body of the storm due to the underrepresented variability. This counteracting effect can result in the misleading outcome of insignificant overall mean biases over the entire storm's area. Although this might be seen as a desirable effect, it is cautioned that it has to be considered carefully as it might lead to undesirable biases in precipitation retrievals if the inversion algorithm does not distinguish between fully and partially covered FOVs, which were shown here to have distinctly different biases. It is emphasized that this study does not mean to imply that any biases found here are to be used directly in a correction of current radiative transfer estimates. Rather, our study provides quantitative estimates of the direction and magnitude of brightness temperature biases occurring from a lack of variability in modeled hydrometeor fields. These biases can be eliminated in different ways. One way is via enhancing the variability of modeled clouds and accounting for partial beamfilling, as explored in this paper.

[35] Further analysis of more storms from different regions is needed to fully assess the partial beamfilling

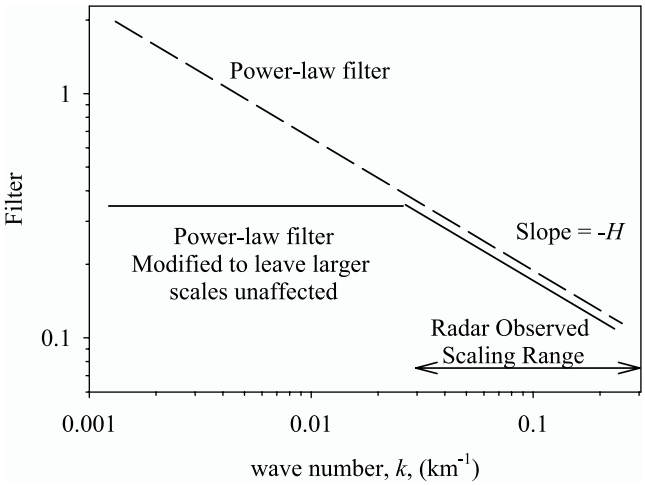

Figure B1. The filter used for fractional integration. The filter is the multiplier in Fourier space. The idea is to leave larger scales, where scaling is not observed, untouched. Fractional differentiation is accomplished with a similar filter but with the slope = $+H$.

problem. Also, observations of hydrometeor species are needed to validate the scaling hypothesis of the statistical properties of these species (this analysis was performed here on the modeled species) and obtain properly validated scaling parameters for 3D downscaling. Although the simple treatment of the vertical structure of hydrometeors in our downscaling seems adequate (see for example the realism in the structure of the vertical profiles of the downscaled fields of *Harris and Foufoula-Georgiou* [2001]), a more elaborate analysis of the vertical structure of hydrometeor species would be beneficial.

Appendix A: Physical Interpretation of Scaling Parameters

[36] The multiscaling parameters C_1, α, and H, characterizing the precipitation fields in this study have physical interpretations discussed elsewhere in the literature [e.g., *Harris et al.*, 2001] and can be used as indicators of intermittency, spikiness and smoothness, respectively. In particular the parameters C_1 and α characterize the intermittency and spikiness of the fluctuations as shown in Figures A1a and A1b, respectively. In Figure A1a, α is kept constant to illustrate the effect of increasing intermittency, C_1, while in Figure A1b, C_1 is kept constant to illustrate the effect of increasing α. The effect of the smoothness parameter, H, is illustrated in Figure A1c, and determines the degree of (fractional) integration required to transform the fluctuations into the real precipitation field.

Appendix B: Cascade-Based Upscaling-Downscaling Technicalities

B1. Zeros

[37] The presence of large areas of zeros between individual rain cells (particularly in multicell convective systems) is a dominant feature of observed rainfall fields. These areas of zero rainfall must be more or less conserved after the upscaling-downscaling procedure. The discrete cascade poses no problem, as a multiplicative weight multiplied by zero is still zero. However a problem occurs when fractionally differentiating the field, as an additive offset may be introduced, which turns areas of zeros into nonzero values. To overcome this problem, any offset introduced by the fractional differentiation must be removed such that areas of zeros remain predominantly zero. This is accomplished by simply establishing a mask identifying the large areas of contiguous zero values in the field before the field is differentiated. After the differentiation, the mask is used to find the mean of the pixels in the differentiated field, which were originally zero before the differentiation. This mean is then subtracted from the original field before the absolute value of the pixels is taken.

[38] This procedure works best when the presence of zeros is predominant (i.e., > 50% zeros) which was the case in all the fields downscaled in this study. In essence, the zeros (which have been so problematic in studies of rainfall which employ cascade based methodologies) are advantageously used to keep track of the absolute levels in the field, which may otherwise be lost.

B2. Modified Fractional Differentiation-Integration

[39] Observed rainfall rarely scales over the full range of observed scales and usually scales from the smallest observable scale up to some maximum scale. Once again, as in the previous section, it is not the actual cascading process that one worries about, since it only acts on the smallest scales, but rather the fractional differentiation and integration process. The fractional differentiation-integration process amounts to a filter which multiplies the Fourier transform of a field by $k^{\pm H}$, $H > 0$, with $+H$ for differentiation and $-H$ for integration [e.g., *Harris et al.*, 2001]. The modification of the filter is shown in Figure B1.

Appendix C: Effect of Spatial Correlation of the Precipitation Field on T_b Computations

[40] A simple experiment can illustrate the effect of spatial correlation of the precipitation field on computed microwave radiance fields. Consider taking a cloud model

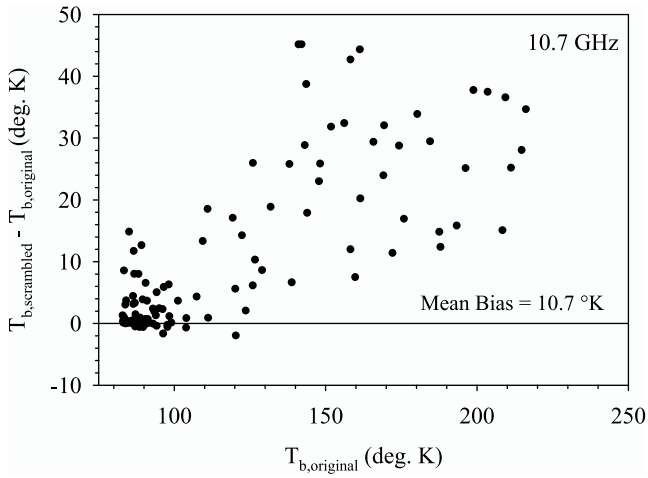

Figure C1. Bias in microwave radiance fields at 10.7 GHz between original field and one with identical variability but pixels randomly scrambled within each 24 × 24 km^2 FOV.

and randomly scrambling the pixels within each nonoverlapping 24×24 km^2 box representing a satellite FOV. This, naturally keeps the CV and the entire distribution identical within each FOV. However, due to nonlinear interactions of microwave radiation within a precipitating atmosphere, the scrambling introduced mean biases of $\sim$10 K in the simulated microwave radiance fields (see Figure C1).

[41] **Acknowledgments.** This work has been supported by the NASA-TRMM program (grant NAG5-7715) and partially by the U.S. Weather Research Program (NSF grant ATM-9714387) and the NOAA/NASA GCIP program (grant NAG8-1519). We wish to thank the National Computation Science Alliance and the University of Minnesota Supercomputing Institute without whose resources and technical assistance, this project would not be possible. Finally, we acknowledge helpful discussions with Shaun Lovejoy of McGill University.

References

Davis, A., A. Marshak, W. Wiscombe, and R. Cahalan, Multifractal characterizations of intermittency in nonstationary geophysical signals and fields: A model based perspective on ergodicity issues illustrated with cloud data, in *Current Topics in Nonstationary Analysis*, edited by G. Treviño et al., pp. 97–158, World Sci., River Edge, N. J., 1996.

Feller, W., *An Introduction to Probability Theory and its Applications*, vol. II, 626 pp., John Wiley, New York, 1966.

Ferrier, B. S., W.-K. Tao, and J. Simpson, A double-momentum multiple-phase four-class bulk ice scheme, part II, Simulations of convective storms in difference large-scale environments and comparisons with other bulk parameterizations, *J. Atmos. Sci.*, *52*(8), 1001–1033, 1995.

Georgakakos, K. P., A. A. Carsteanu, P. L. Sturdevant, and J. A. Cramer, Observation and analysis of midwestern rain rates, *J. Appl. Meteorol.*, *33*, 1433–1444, 1994.

Gorenflo, R., and F. Mainardi, Fractional calculus and stable probability distributions, *Arch. Mech.*, *50*(3), 377–388, 1998.

Harris, D., Multifractal properties of rainfall: Methods and interpretation, Ph.D. thesis, Univ. of Auckland, Auckland, 1998.

Harris, D. H., and E. Foufoula-Georgiou, Subgrid variability and stochastic downscaling of modeled clouds: Effects on radiative transfer computations for rainfall retrieval, *J. Geophys. Res.*, *106*, 10,349–10,362, 2001.

Harris, D., M. Menabde, A. Seed, and G. L. Austin, Multifractal characterization of rain fields with a strong orographic influence, *J. Geophys. Res.*, *101*, 26,405–26,414, 1996.

Harris, D., A. W. Seed, M. Menabde, and G. L. Austin, Factors affecting multiscaling analysis of rainfall time series, *Nonlinear Proc. Geophys.*, *4*(3), 137–156, 1997.

Harris, D., E. Foufoula-Georgiou, K. Droegemeier, and T. Levit, Multiscale statistical properties of a high-resolution precipitation forecast, *J. Hydrometeorol.*, *2*(4), 406–418, 2001.

Hilfer, R., Fractional derivatives in static and dynamic scaling, in *Scale Invariance and Beyond*, edited by B. Dubrulle, F. Graner, and D. Sornette, Springer-Verlag, New York, 1997.

Krajewski, W., E. N. Anagnostou, and G. J. Ciach, Effects of the radar observation process on inferred rainfall statistics, *J. Geophys. Res.*, *101*, 26,493–26,502, 1996.

Kummerow, C., Beamfilling errors in passive microwave rainfall retrievals, *J. Appl. Meteorol.*, *37*, 356–370, 1998.

Kummerow, C., W. Barnes, T. Kozu, J. Shiue, and J. Simpson, The Tropical Rainfall Measuring Mission (TRMM) sensor package, *J. Atmos. Oceanic Technol.*, *15*(3), 809–817, 1998.

Lin, Y., R. D. Farley, and H. D. Orville, Bulk parameterization of the snow field in a cloud model, *J. Appl. Meteorl.*, *22*, 1065–1092, 1983.

Liu, Q., C. Simmer, and E. Ruprecht, Three-dimensional radiative transfer effects of clouds in the microwave spectral range, *J. Geophys. Res.*, *101*, 4289–4298, 1996.

Lovejoy, S., D. Schertzer, Multifractals and rain, in *New Uncertainty Concepts in Hydrology and Water Resources*, edited by A. W. Kundzewicz, pp. 61–103, Cambridge Univ. Press, New York, 1995a.

Lovejoy, S., and D. Schertzer, How bright is the coast of Brittany?, in *Fractals in Geoscience and Remote Sensing, Image Understanding Research*, vol. 1, edited by G. Wilkinson, I. Kanellopoulos, J. Mégier, pp. 102–151, Inst. for Remote Sens. Appl., Brussels, Belguim, 1995b.

Matrosov, S. Y., and I. V. Djalalova, Spatial variability of stratiform precipitation estimated from the X-band radar measurements, paper presented at 30th International Conference on Radar Meteorology, Am. Meteorol. Soc., Munich, Germany, 2001.

Menabde, M., A. W. Seed, D. Harris, and G. L. Austin, Self-similar random fields and rainfall simulation, *J. Geophys. Res.*, *102*, 13,509–13,515, 1997.

Pecknold, S., S. Lovejoy, D. Schertzer, C. Hooge, and J. F. Malouin, The simulation of universal multifractals, in *Cellular Automata:Prospects in Astrophysical Applications*, edited by J. M. Perdang and A. Lejeune, pp. 228–267, World Sci., River Edge, N. J., 1993.

Perica, S., and E. Foufoula-Georgiou, Model for multiscale disaggregation of spatial rainfall based on coupling meteorological and scaling descriptions, *J. Geophys. Res.*, *101*, 26,347–26,361, 1996.

Roberti, L., J. Haferman, and C. Kummerow, Microwave radiative transfer through horizontally inhomogeneous precipitating clouds, *J. Geophys. Res.*, *99*, 16,707–16,718, 1994.

Samorodnitsky, G., and M. S. Taqqu, *Stable Non-Gaussian Random Processes*: *Stochastic Models with Infinite Variance*, 632 pp., Chapman and Hall, New York, 1994.

Schertzer, D., and S. Lovejoy, Physical modeling and analysis of rain and clouds by anisotropic scaling multiplicative processes, *J. Geophys. Res.*, *92*, 9693–9714, 1987.

Schertzer, D., and S. Lovejoy, Hard and soft multifractal processes, *Physica A*, *185*, 187–194, 1992.

Tessier, Y., S. Lovejoy, and D. Schertzer, Universal multifractals: Theory and observations for rain and clouds, *J. Appl. Meteorol.*, *32*, 223–250, 1993.

Wilson, J., D. Schertzer, and S. Lovejoy, Physically based modelling by multiplicative cascade processes, in *Scaling, Fractals and Non-linear Variability in Geophysics*, edited by D. Schertzer and S. Lovejoy, pp. 185–208, 1991.

Xue, M., K. K. Droegemeier, V. Wong, A. Shapiro, and K. Brewster, Advanced Regional Prediction System (ARPS), version 4.0 user's guide, Cent. for Anal. and Predict. of Storms (CAPS), Univ. of Okla., Norman, 1995.

E. Foufoula-Georgiou and D. Harris, St. Anthony Falls Laboratory, University of Minnesota, Mississippi River at 3rd Avenue S.E., Minneapolis, MN 55414, USA. (efi@tc.umn.edu)

C. Kummerow, Department of Atmospheric Sciences, Colorado State University, Fort Collins, CO 80523, USA.